Arch. Metall. Mater. **63** (2018), 3, 1249-1256

DOI: 10.24425/123798

Z. LIANG*#, Y. GUI*, Q. ZHAO*

INVESTIGATION OF MICROSTRUCTURES AND MECHANICAL PROPERTIES OF T92 MARTENSITIC STEEL/SUPER304 AUSTENITIC STEEL WELD JOINTS MADE WITH THREE WELDING CONSUMABLES

The microstructures and mechanical properties of T92 martensitic steel/Super304 austenitic steel weld joints with three welding consumables were investigated. Three types of welding materials ERNiCr-3, ERNiCrCoMo-1and T-304H were utilized to obtain dissimilar welds by using gas tungsten arc weld (GTAW). The results show that heat affect zone (HAZ) of T92 steel consists of coarse-grained and fine-grained tempered martensites. The microstructures of joints produced from ERNiCrCoMo-1 consist of equiaxed dendrite and columnar dendrite grains, which are more complicated than that of ERNiCr-3. In the tensile tests, joints constructed from ERNiCrCoMo-1 and T-304H met the ASME standard. The highest fracture energy was observed in specimens with the welding material ERNiCrCoMo-1. Ni content in weld seam of ERNiCrCoMo-1 was highest, which was above 40%. In conclusion, the nickel alloy ERNiCrCoMo-1 was the most suitable welding material for joints produced from T92 martensitic steel/Super304 austenitic steel.

Keywords: Dissimilar welding, Welding materials, Microstructures, Mechanical properties

1. Introduction

Developing supercritical and ultra-supercritical power boilers are effective ways to improve fossil utilization and to reduce carbon dioxide emission [1]. In the steam system of power plants, steam temperature and pressure gradually increase. Corresponding materials are utilized to parts with respect to steam parameters [2,3]. For example, final super-heaters with a steam temperature of 605°C are made of materials such as Super 304H, TP347HFG, or HR3C steel [2-5], whereas secondary superheaters with a steam temperature of 560°C are constructed with materials such as T91, T92, or E911 steel [6-12]. Therefore, dissimilar steel welding is inevitable. In severe environments, the economical operation of power plants for a long period depends on dissimilar welding joints [13,14].

Several institutions reported that the life of dissimilar steel joints is shorter than the expected design life [15-17]. This phenomenon may be caused by the welding material because the migration of the carbon element results in the early failure of welded joints [15,16]. The early failure or the failure probability of welding joints produced from nickel-based welding materials occurred much later than those joints made with austenitic welding material [17]. Moreover, the failure probability is quite small when nickel-based welding materials are utilized.

Shamanian studied the microstructures and mechanical properties of A335 stainless steel/347 low-alloy steel dissimilar steel joints. The results showed that ERNiCr-3 was more suitable as welding material compared with 347/A335 dissimilar steel. Moreover, Inconel 617/310 stainless steel welding materials were compared with each other. The result indicated that Inconel 617 was better than Inconel82 and 310 [18,19]. Hwa-Teng and Lee reported the influence of composition welding materials on the welding of alloy 690 [20]. Yang and Tang respectively investigated the microstructures and mechanical properties of T92 martensitic steel/Super304 austenitic steel weld joints at room temperature and after aging treatment [21-24]. At room temperature, ERNICr-3 was favorable as a welding material, whereas ERNiCrMo-3 was favorable after aging treatment. However, studies on comparison of welding materials ERNiCr-3, ERNiCrCoMo-1and T-304H for T92 martensitic steel/Super304 austenitic steel are still lacking. Therefore, this study on welding materials is significant and necessary [25].

Ni-based welding consumables ERNiCr-3 and ERNiCrCoMo-1 and stainless steel consumable T-304H were used to obtain the best welding material for T92/Super 304H dissimilar steel weld by analyzing their microstructures and mechanical properties.

2. Experimental materials and methods

T92 and Super 304H steel tubes with sizes of Φ51 mm×13 mm were selected for the experiment, and their corresponding chemical compositions, in accordance with ASME standards, are listed

* XI'AN JIAOTONG UNIVERSITY, SCHOOL OF ENERGY AND POWERENGINEERING, KEY LABORATORY OF THERMAL FLUID SCIENCE AND ENGINEERING OF MOE, XI'AN 710049, PR CHINA

Corresponding author: liangzy@xjtu.edu.cn

TABLE 1

Chemical compositions of investigated materials (wt. %)

Materials	C	Cr	Mo	V	Nb	Ni	Mn	P	S	Si	W	Cu
T92	0.11	9.0	0.50	0.23	0.06	0.26	0.46	0.015	0.002	0.40	1.64	/
S304H	0.09	18.33	/	/	0.50	8.90	0.80	0.03	0.001	0.025	/	2.94

TABLE 2

Chemical compositions of welding materials (wt. %)

Materials	C	Mn	Si	P	S	Cr	Ni	Co	Mo	Cu	Al	Ti
ERNiCr-3	0.031	2.80	0.04	0.004	0.002	20	69.5	/	/	0.02	/	0.35
ERNiCrCoMo-1	0.09	0.06	0.6	0.006	0.002	22	55.6	12.4	9.5	0.03	1.0	0.15
T-304H	0.09	3.46	0.32	0.012	0.003	18.5	15.9	/	0.80	3.00	/	/

TABLE 3

Primary welding parameters in each welding pass

Pass No.	Current (A)	Volt (V)	Welding speed (mm/min)	Heater current (A)
1	350	12.4	75	36
2	350	13	74	38
3	330	12.6	71	15

in Table 1. The heat treatment of two steels is described below: 1) T92 steel: normalized at 1040°C and tempered at 760°C; 2) Super304H steel: solution treatment at 1150°C followed by water cooling to room temperature. The ERNiCr-3, ERNiCrCoMo-1, and T-304H welding materials with a φ1 mm specification were selected, and their chemical compositions are shown in Table 2. T92/Super 304H dissimilar steel welds were obtained using gas tungsten arc weld (GTAW), and the parameters of GTAW are g in Table 3. Figure 1 shows the schematic diagram of T92/SUPER 304H dissimilar steel welds with a typical "V" groove. After welding, post-welding heat treatment was carried out for 2 h to stabilize the microstructures and to eliminate the residual stress, as showed in Figure 2.

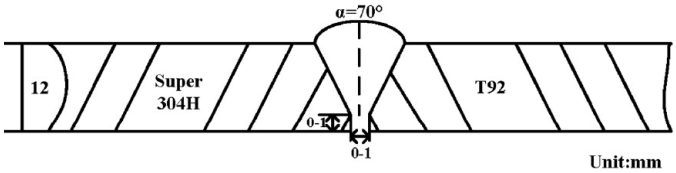

Fig. 1. Schematic diagram of welding process of T92/Super 304H dissimilar weld joints

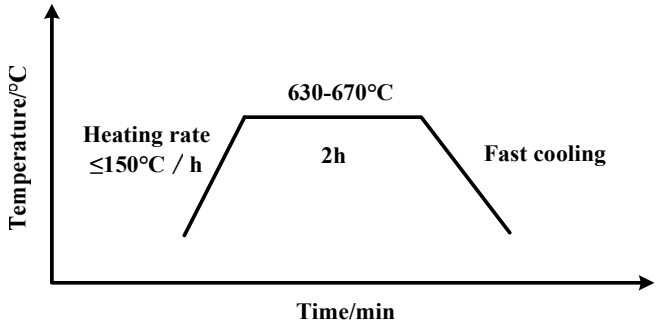

Fig. 2. Schematic diagram of post welding heat treatment

After non-destructive X-ray and penetration tests, tension and impact specimens were manufactured to determine the mechanical properties of T92/Super 304H dissimilar steel welds. Impact and tensile tests on T92/Super 304H dissimilar steel welds were carried out respectively at room temperature according to ASTM E23-02a and E8-04 standards. SANS and XYB305C were used for the tensile and impact tests. A VH-5DC hardness tester was used for the hardness test.

An OLYMPUS GX4 optical microscope was used to observe the metallurgical structure of these joints. Three etching solutions were used as follows: 1) T92: Picric acid 5 mL, ethanol 40 mL; 2) Super 304H: $CuSO_4$4g, HCl 20 mL, ethanol 20 mL; 3) weld seam: aqua regia. A JED 2200 scanning electron microscope was used to obtain the microstructures and the tensile and impact fracture of these joints. An energy dispersive spectroscopy (EDS) was performed to determine the elements in the weld seam and the main metallic elements in the precipitated particles.

3. Results and discussion

3.1. Microstructures of dissimilar joints

Figure 3a shows the microstructure of T92 base metal. It consists of tempered martensite with secondary phase particles along the lath martensites and the austenite grain boundaries. The composition of these particles was characterized via EDS. The results illustrate that the particles are mainly carbides, as showed in Figure 3d and Figure 3e. W content in Figure 3d is higher than that in Figure 3e, thereby indicating that the particles (Laves) along the boundaries are distinct from the particles (MX) in the grains. The microstructure of the Super 304H base metal is composed of equiaxed austenitic grains with an average size

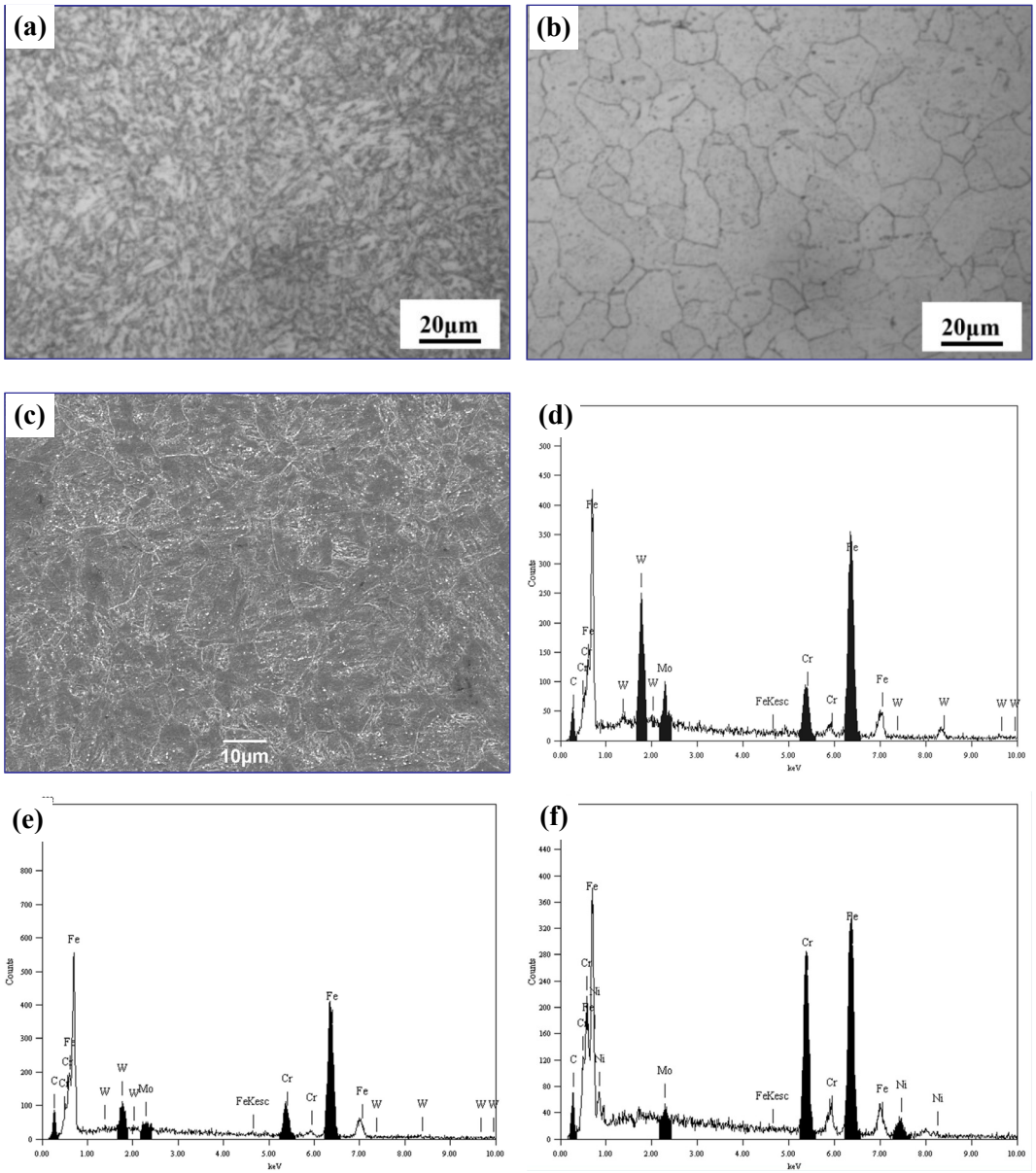

Fig. 3. Microstructures of base metals (a) T92 base metal (b) Super 304H base metal (c) T92 base metal (d) EDS result of second-phase particles at the grain boundary of T92 (e) EDS result of second-phase particles in the grain of T92 (f) EDS result of second-phase particles at the grain boundary of Super 304H base metal

of 15 μm. Secondary phase particles, which are mainly $M_{23}C_6$ (M = Fe, Cr, Mo), are distributed along the grain boundaries and in the austenite grains, as shown in Figure 3f.

Figure 4a-c shows the microstructure of the T92 steel HAZ near the weld metal. Coarse-grain (CG) and fine-grain (FG) HAZs were observed in this region. The average sizes of CG and FG are 22 μm and 12 μm, respectively. The grain size of CGHAZ is larger than that of the base metal, and the grain size of FGHAZ is less than that of base metal. The discrepancy in grain sizes in the HAZ is related to the horizontal distribution of high temperature in the welding process. The welding temperature of FG is close to the austenitizing temperature AC_3, whereas the welding temperature of CG is higher than the austenitizing temperature AC_3, thereby leading to austenite-martensite phase transformation. As saw in Figure 4, the fusion line between the T92 base metal and the weld metal is clear. Delta ferrite phases were observed in the T92 CGHAZ when elding material used was ERNiCr-3 and T-304H. By contrast, the delta phase was not observed when weld material used was ERNiCrCoMo-1, as showed in Figure 4b. Delta ferrite phases in T92 CGHAZ have a detrimental effect on the mechanical properties of the weld joints and cause creep-cracking in T92 HAZ.

Figure 4d-f shows the microstructure of Super304H HAZ produced from three types of welding materials. The microstructure only consists of coarse austenitic grains with an average size of 30 μm, which is larger than that of the Super 304H base metal. The temperature of Super 304H HAZ was lower than the austenitic phase transformation temperature during the processing of GTAW, which indicates that the base metal only absorbs heat during grain growth. Along the grain boundaries and in the grains, the secondary phase particles were similar to those in the Super304H base metal. As seen in Figure 4f, coarsening of grain

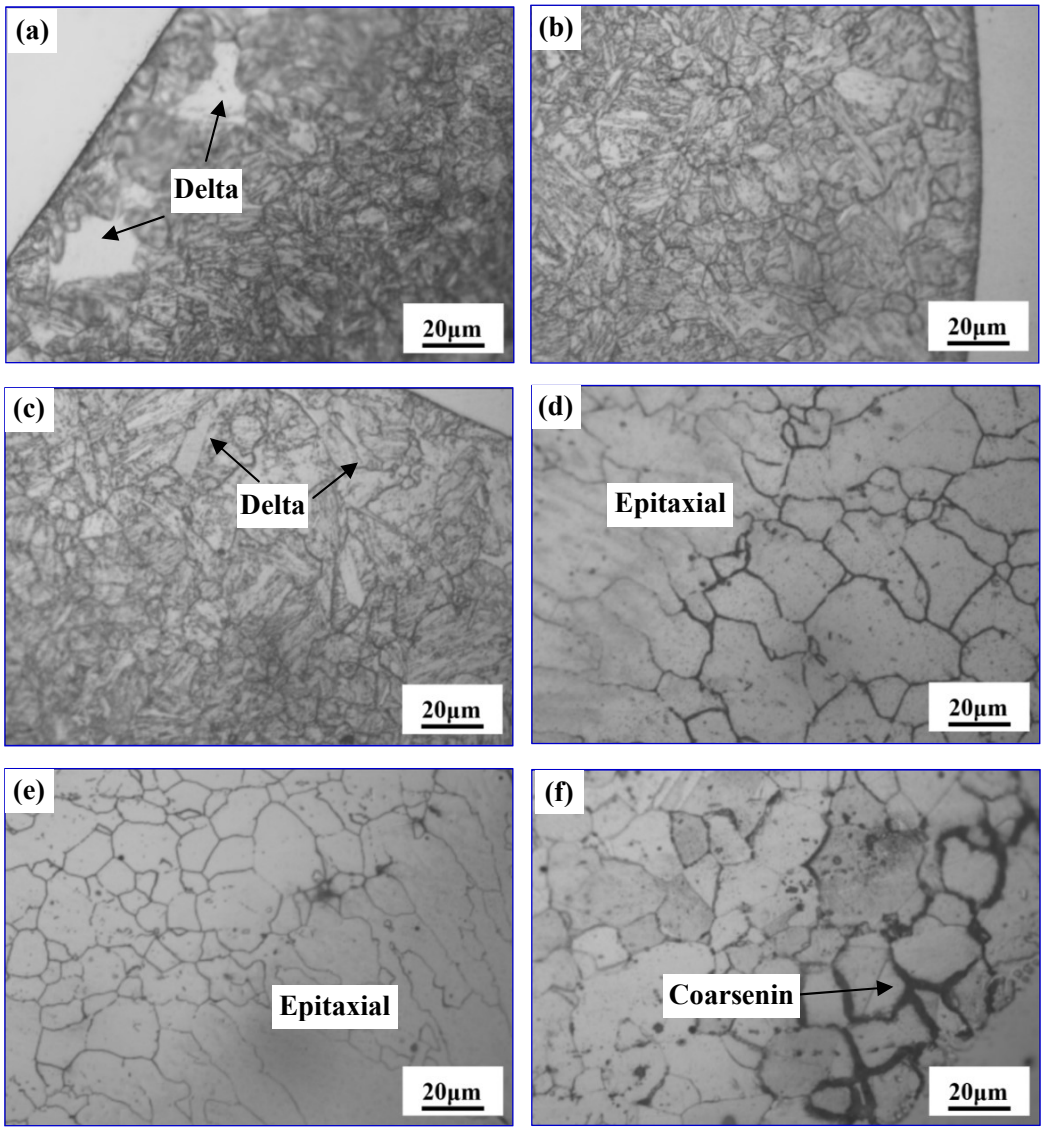

Fig. 4. Metallurgical pictures of T92 HAZ and Super 304H HAZ; (a) ERNiCr-3 (b) ERNiCrCoMo-1 (c) T-304H (d) ERNiCr-3 (e) ERNiCrCoMo-1 (f) T-304H

boundaries in Super304H HAZ is distinct. Furthermore, when welding materials used were ERNiCrCoMo-1 and ERNiCr-3, epitaxial growth was observed at the fusion line between Super 304H HAZ and weld seam, as showed in Figure 4e and Figure 4d.

Figure 5 shows the microstructure of the weld seam. The microstructures of the weld seam were entirely austenite, which is in accordance with the location in the Schaeffer Figure [26]. The formation of an entirely austenite structure is due to the high content of Ni in the welding materials, as listed in Table 4. Ni promotes the formation of the austenite phase by expanding the austenite phase field.

Figure 5a shows the microstructures of the weld seam containing a single axis dendrite and a large number of solidification sub-grain boundaries. Solidified sub-grains grew along the crystallization direction at [100] during the solidification process [26]. Therefore, the dislocation density of the sub-grain boundary is low. The microstructures of the welding material ERNICrCoMo-1 is comprised of equiaxed and non-equiaxed dendrites. Solidification grain boundary (SGB) and migrated

TABLE 4

Calculated value of Nieq and Creq of welding materials and base metal(%)

	ERNiCr-3	ERNiCrCoMo-1	T-304H	T92	Super304H
Ni_{eq}	71.83	58.33	20.33	3.79	12.00
Cr_{eq}	20.76	32.7	19.78	10.13	18.62

grain boundary (MGB) are observed in Figure 5c. The segregation of secondary phase particles from the Ni-based welding materials reveal carbides containing Ti and Cr and were columnar and ellipsoid in shape, as showed in Figure 5b. Compared to the Mo and Co in the welding material ERNiCr-3, that in ERNiCrCoMo-1 has an important function in enhancing the yield and tensile strength of the weld metal [26].

The microstructures of the weld metal made from austenitic materials were skeletal ferrite and austenitic with a FA solidification mode. The weld cooling rates were moderate or had a low Creq/Nieq. Nevertheless, these values were still within

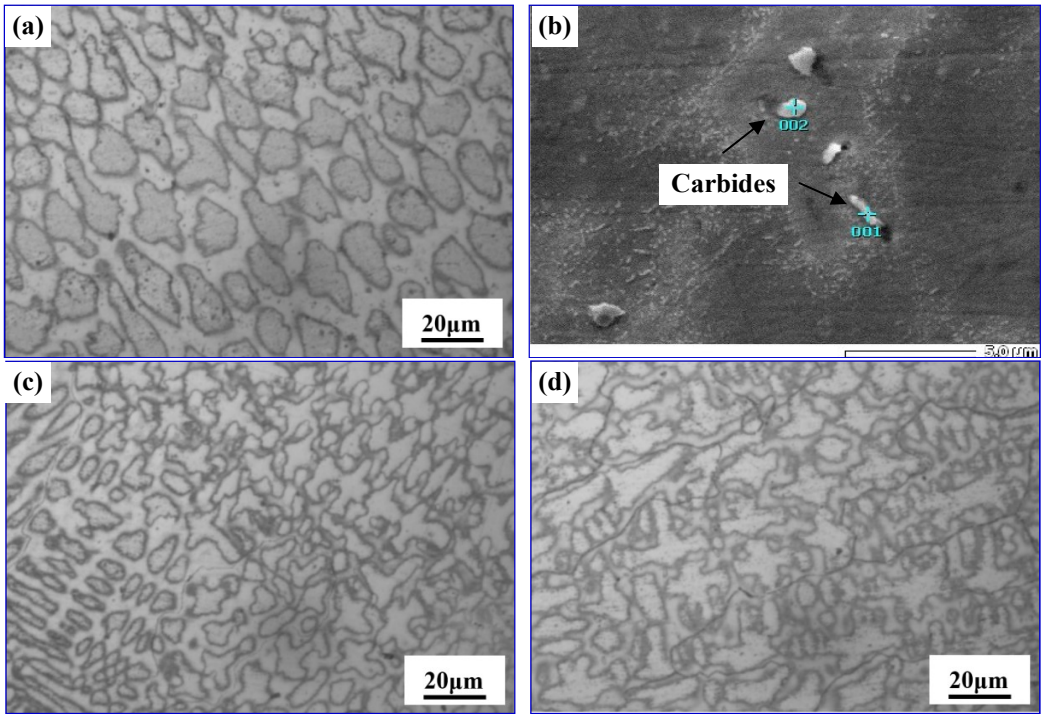

Fig. 5. Metallurgical pictures of weld seam produced by three welding materials (a) ERNiCr-3 (b) ERNiCr-3 secondary phase particles (c) ERNiCrCoMo-1 (d) T-304H

the FA range, which results in a skeletal ferrite morphology. Numerous SGBs and MGBs can be observed in Figure 5d. The formation of MGBs is due to the low solidification energy along a perpendicular direction. Given the lack of segregated elements such as Ti/Mo/Nb, the welding material is composed of Fe, Ni, and Cr, which are known for their low tendency to segregate at the grain boundaries. As a result, the solidification cracking of T-304H joints is less sensible than that of Ni-based welding materials. However, in a high temperature and pressure environment, the austenitic welding material could not effectively prevent the migration of C, which results in the formation of a softened zone in the HAZ and leads to the premature failure of the welded joints [15].

3.2. Mechanical properties

Table 5 shows that the welded joints produced from welding materials ERNiCrCoMo-1 and T-304H meet the tensile strength standards of ASME P92 and Super 304H steel. Fractures positions of welded joints produced from ERNiCr-3 and ERNiCrCoMo-1 were located at the weld seam. These locations were caused by the sensitive solidification cracking of fully austenitic structures. The tensile strength of joints produced from ERNiCr-3 was minimum, thereby indicating that the weld metal is the weakest part in T92/SUPER 304H dissimilar steel joints. This result can be attributed to the precipitation of secondary phase particles and the low density dislocation because of concentrated stresses on round second phase particles and micro-crack aggregates, which grew as the micro-cracks extended. Thus, the weld seam is significantly weakened. Comparing the welding materials ERNiCr-3 and ERNiCrCoMo-1, the latter has a higher tensile strength because of the dispersion-strengthening effect of Mo and Co [26]. Mo is prone to form carbides at high temperatures, which can increase the tensile strength of the weld seam. The tensile strength of T-304H weld is the highest and the fracture location is at the T92 base metal because the composition of the welding material T-304H is similar to that of the Super 304H base metal. Fusion with Super 304H base metal is also easier compared to fusion with the other two Ni-based welding materials.

TABLE 5

Results of tensile experiment

Welding materials	Tensile strength /Mpa	Neck	Rupture position
ERNiCr-3	635	Slight	Weld seam
	632	Slight	Weld seam
ERNiCrCoMo-1	658	Slight	Weld seam
	655	Slight	Weld seam
T-304H	689	serious	T92 base metal
	689	serious	T92 base metal
ASME T92	≥620	/	/
ASME S304H	≥655	/	/

Figure 6 shows the tensile fractures of T92 martensitic steel/ Super304H austenitic steel weld joints. All fractures are ductile, as saw from the fracture morphology. In Figure 6a, numerous fine equiaxed dimples with distinct tearing ridges can be observed in the fracture. Figure 6c shows a large number of secondary cracks. Figure 6d and Figure 6e show the central fiber zone and radiation zone in the tensile fractures with secondary cracks, respectively. Secondary cracks have a relationship with grain

boundary sliding, which results in the formation of a w-type hollow at the intersection of three grain boundaries. Tearing ridges in the central fiber zone are soft. The dimple in Figure 6d is larger and deeper than those in Figure 6b and 6f. Therefore, welded joints made from ERNiCrCoMo-1 are better than those made from ERNiCr-3 depended on their microstructures. Figure 6f shows the uneven regular central fiber zone and the radiation zone with secondary cracks.

Figure 7 shows that the impact-absorbing energy of the weld seam, and the HAZ meets ASME standard requirements (41J). The maximum and minimum impact-absorbing energy are observed in the Super 304H HAZ and weld seam, respectively.

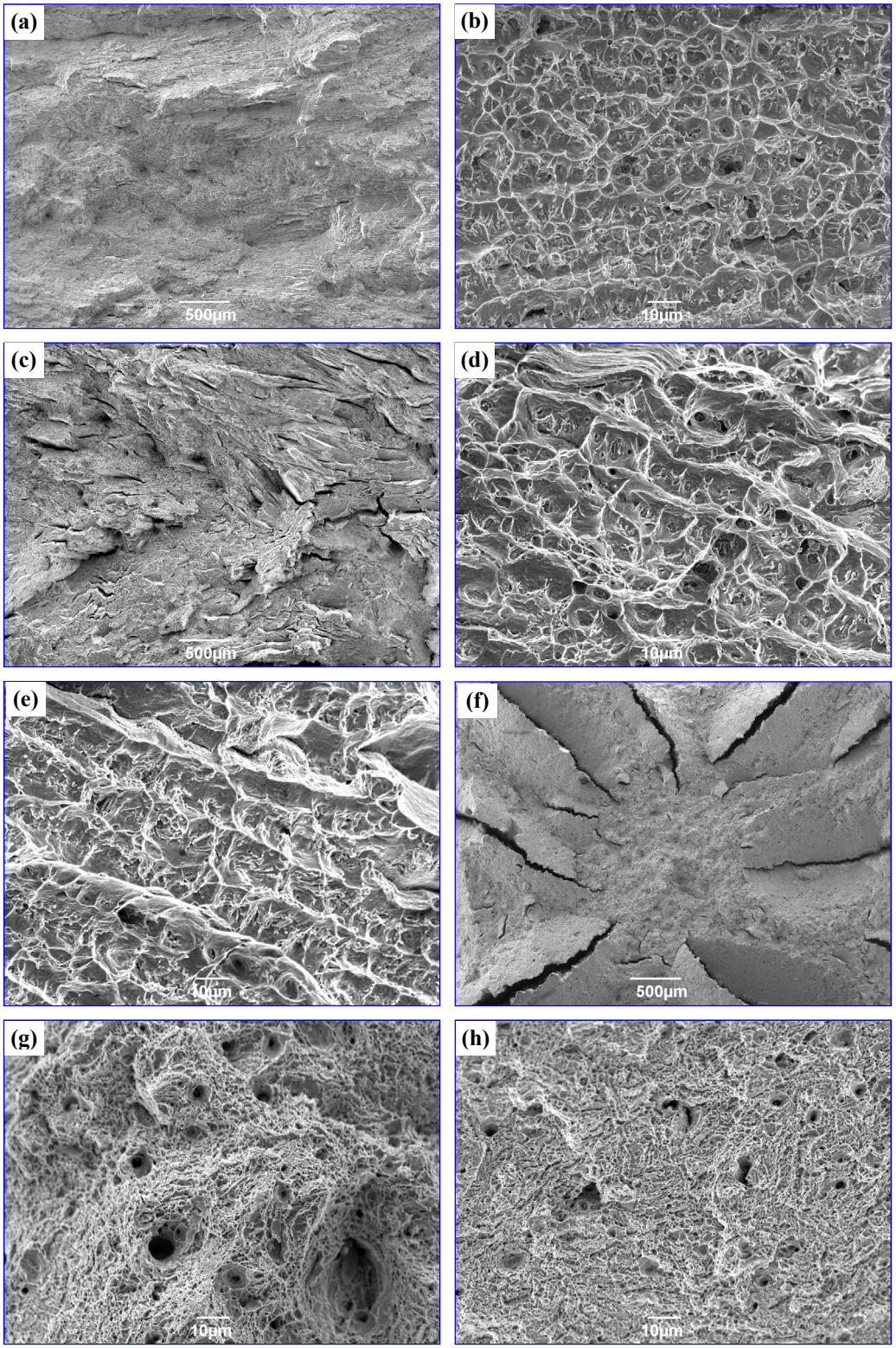

Fig. 6. Tensile fractures of weld joints with three welding materials (a) surface morphology of ERNiCr-3 (b) central fiber zone of ERNiCr-3 (c) surface morphology of ERNiCrCoMo-1 (d) central fiber zone of ERNiCrCoMo-1 (e) radiation zone of ERNiCrCoMo-1 (f) T-304H (g) central fiber zone of T-304H (h) radiation zone of T-304H

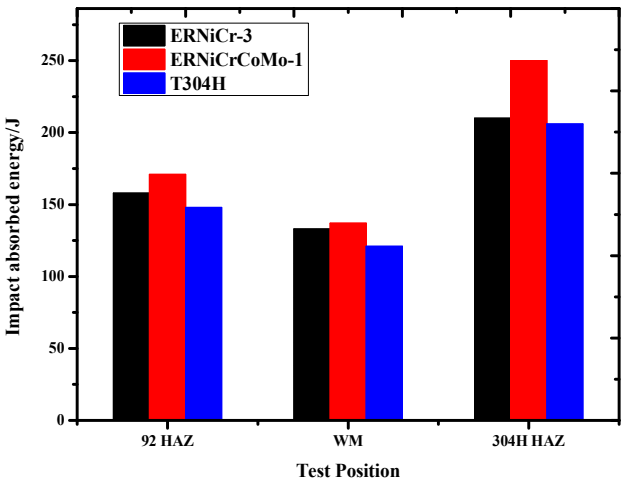

Fig. 7. Impact absorbing energy of welding joints

As showed in Figure 8a, apparent ladders were observed in the fracture morphology of the weld seam produced from ERNiCr-3. Figure 8a is a magnified image of Figure 8b, and the former shows that tiny dimples were visible and that the absorbed energy of the secondary cracks of ERNiCr-3 weld joints were significantly higher than those of the other two weld materials. The additive of Co in ERNiCrMo-1 improved the impact toughness.

Figure 9 displays that the hardness values of dissimilar steel joints made from three types of welding consumables were consistent. The overall decreasing trend in the hardness value is as follows: T92HAZ, T92BM, S304BM and S304HHAZ. During the welding process, T92 HAZ undergoes an austenite-martensitic transformation and forms a hardened martensitic structure, which results in a high hardness value. Hence, this study effectively used post-weld heat treatment to reduce the hardness of the HAZ. The minimum hardness value was obtained and the coarse austenite structure where the weld and shape of the precipitated second phase particles was observed because the hardness of the material was strengthened when it was in close contact with the second phase. High hardness values often result in the decrease in toughness of the material in applications, which results in the brittle fracture of welded joints. The tensile strength and hardness values of welded joints produced from ERNiCrCoMo-1 are higher than those of ERNiCr-3 because of the solid-solution strengthening effect of Mo and the dispersion strengthening effect of its carbides.

Figure 10 shows Ni content across the weld seam of three welding joints, which is a critical parameter to evaluate the welding joints. It is reported that welding joints with Ni content above 40% perform excellent oxidation and corrosion resistance at elevated temperatures. Ni content of welding joint produced

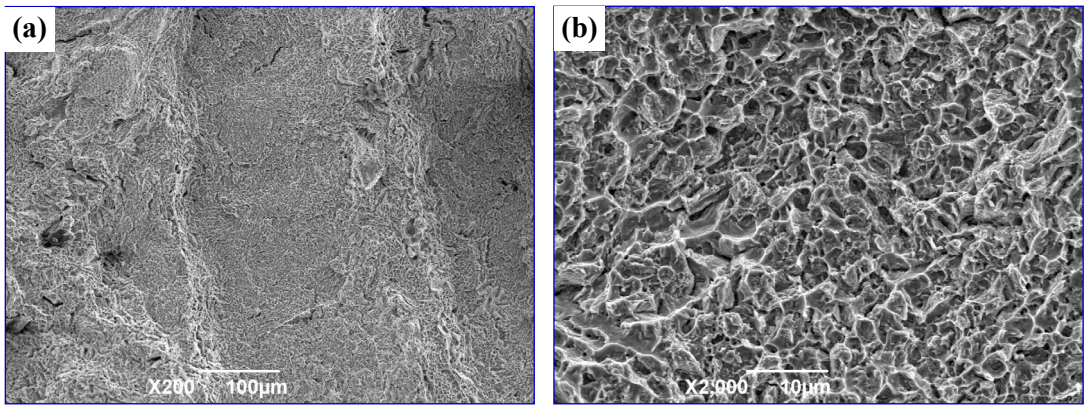

Fig. 8. Fracture appearances of joints; (a) Fracture appearances (low magnification) (b) Fracture appearances (high magnification)

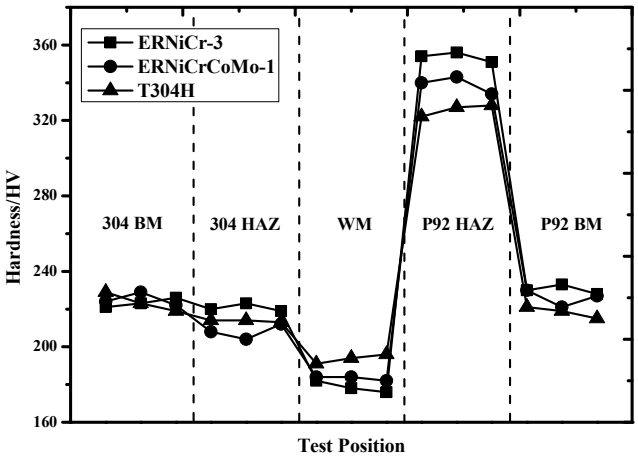

Fig. 9. Micro-hardness profiles across the welds with three welding consumables

with ERNiCoMo-1, which exceeds 40%, is slightly higher than that of other consumables. This indicates that dilution rate of the weld seam is improved using ERNiCoMo-1 as the consumable for T92 and Super 304H.

Finally, considering superior tensile strength, hardness of welding joints and control of dilution rate in weld seam, weld consumable ERNiCrCoMo-1 is the most suitable welding materials for T92 martensitic steel/Super304 austenitic steel weld joints.

4. Conclusions

(1) HAZ of T92 steel consisted of coarse and fine-tempered martensites, whereas HAZ of Super 304H steel was austenitic. In addition to equiaxed dendrites in the microstructures

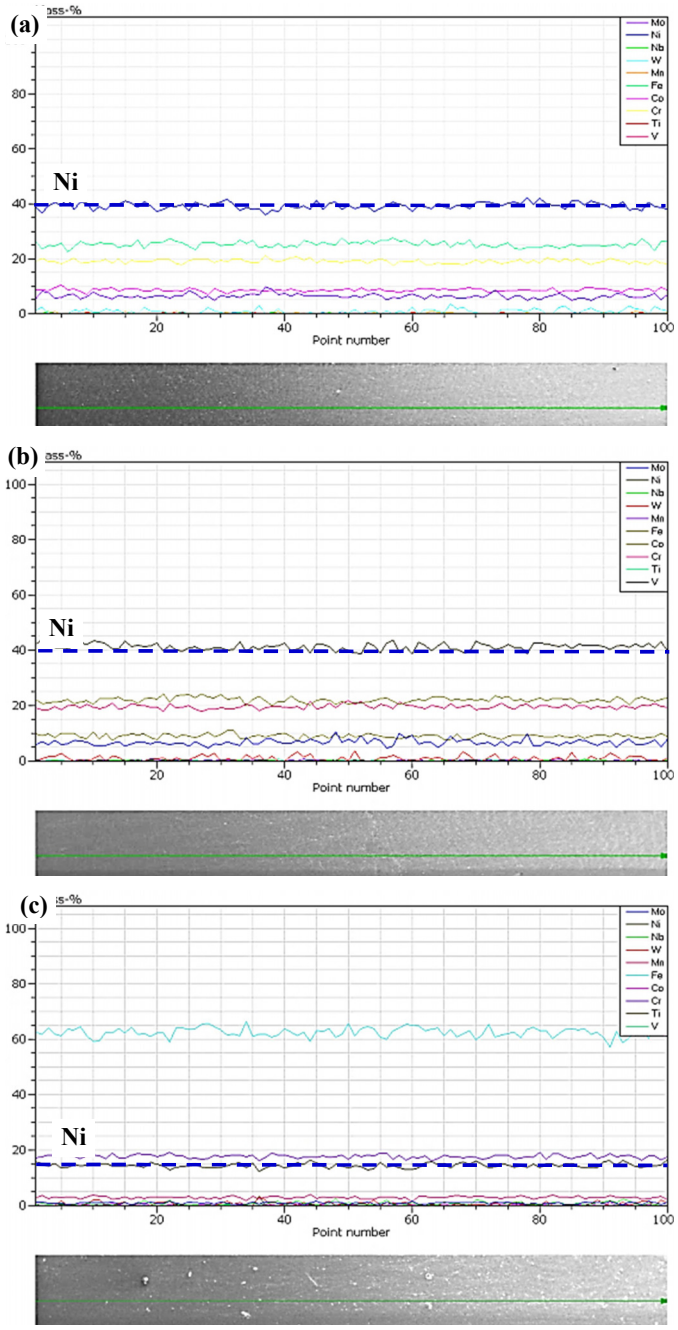

Fig. 10. Ni content in the weld seam (a) ERNiCr-3 (b) ERNiCrCoMo-1 (c) T-304H

of joints produced from ERNiCrCoMo-1 and ERNiCr-3, columnar dendrite grains were also found in ERNiCrCoMo-1.

(2) Welding joints produced from ERNiCrCoMo-1 and T-304H materials met the tensile strength standards of ASME T92 and Super 304H steels. The weld seam was the weakest position of welding joints produced from Ni-based welding materials.

(3) The high impact-absorbing energy of welding joints was observed in the welding material ERNiCrCoMo-1. Given the control of Ni content in the weld seam, superior tensile strength and hardness of welding joints, ERNiCrCoMo-1 materials are the most suitable welding materials for T92 martensitic steel/Super304 austenitic steel weld joints.

Acknowledgements

This work was financially supported by the National Key Research and Development Program of China (No.2016YFC0801904) and the Fundamental Research Funds for the Central Universities the Postdoctoral Funds (2017M620451, 2018T111062), the Shaanxi Province Postdoctoral Research Grant (2017BSHEDZZ41). We would like to thank anonymous reviewers for their helpful comments and suggestions in improving the paper.

REFERENCES

[1] R. Viswanathan, K. Coleman, U. Rao, Int. J. Pres.Ves. Pip. **83** (11), 778-783 (2006).

[2] A. Iseda, H. Okada, H. Semba, M. Igarashi, Energy Mater. **2** (4), 199-206 (2007).

[3] T. Sourmail, Mater.Sci.Tech. **17** (1), 1-14 (2001).

[4] J. Jiang, L. Zhu, Mater. Sci. Eng.A-Struct. **539**, 170-176 (2012).

[5] A. Di Schino, J.M. Kenny, M.G. Mecozzi, M. Barteri, J. Mater. Sci. **35** (19), 4803-4808(2000).

[6] P.J. Ennis, A. Zielinska-Lipiec, O. Wachter, A. Czyrska-Filemonowicz, Acta Mater. **45** (12), 4901-4907 (1997).

[7] V. Sklenička, K. Kuchařová, M. Svoboda, Mater.Charact. **51** (1), 35-48 (2003).

[8] K. Sawada, K. Kubo, F. Abe, Mater. Sci. Eng. A-Struct. **319**, 784-787 (2001).

[9] F. Abe, Sci. Technol. Adv. Mat. **9** (1), 013002 (2008).

[10] F. Abe, T. Horiuchi, M. Taneike, K. Sawada, Mater. Sci. Eng. A-Struct. **378** (1), 299-303 (2004).

[11] K. Kimura, K. Sawada, H. Kushima, K. Sawada, Int. J. Mater. Res. **99** (4), 395-401 (2008).

[12] Y.I. Gong, J. Cao, L.N. Ji, C. Yang, C. Yao, Fatigue Fract. Eng. M. **34** (2), 83-96 (2011).

[13] A. Celik, A. Alsaran, Mater. Charact. **43** (5), 311-318 (1999).

[14] A. Výrostková, V. Homolova, J. Pecha, M. Svoboda, Mater. Sci. Eng. A-Struct. **480** (1), 289-298 (2008).

[15] S. Missori, C. Koerber, Weld. J. **76** (3), 125-134 (1997).

[16] F. Gauzzi, S. Missori, J. Mater. Sci. **23** (3), 782-789 (1988).

[17] C.D. Lundin, Weld. J. **61** (2), 58-63 (1982).

[18] I. Hajiannia, M. Shamanian, M. Kasiri, Mater. Des. **50**, 566-573 (2013).

[19] R. Dehmolaei, M. Shamanian, A. Kermanpur, Mater. Charact. **59** (10), 1447-1454 (2008).

[20] T.Y. Kuo, H.T. Lee, Mater. Sci. Eng. A-Struct. **338** (1), 202-212 (2002).

[21] J. Cao, Y. Gong, K. Zhu, Mater. Des. **32** (5), 2763-2770 (2011).

[22] G. Chen, Q. Zhang, J. Liu, Mater. Des. **44**, 469-475 (2013).

[23] J. Cao, Y. Gong, Z.G. Yang, Int. J. Pres. Ves. Pip. **88** (2), 94-98 (2011).

[24] L. Falat, A. Výrostková, V. Homolová, M. Svoboda, Eng. Fail. Anal. **16** (7), 2114-2120 (2009).

[25] L. Falat, V. Homolová, J. Kepič, M. Svoboda, J. Min. Metall. B. **48** (3), 461-469 (2012).

[26] S. Kou, Welding metallurgy, 2003 Wiley.